Nanopore-Based Sensors

DOI: 10.1002/anie.201200688

DNA Origami Gatekeepers for Solid-State Nanopores**

Ruoshan Wei, Thomas G. Martin, Ulrich Rant, and Hendrik Dietz**

Molecular self-assembly with DNA enables the construction of soluble objects with nanometer to micrometer scale absolute dimensions and custom chemical features,[1] including crystals,[2] patterns,[3] bricks,[4] boxes,[5] and curved shapes,[6] that can open novel paths to scientific discovery.[7] Herein, we report on DNA nanoplates for nanopore-based sensing approaches. Nanopores in biological or solid-state membranes offer great potential for label-free single-molecule sensing applications.[8] Biological nanopores, such as alpha-hemolysin, can be customized within the limits of protein engineering.[9] Artificial nanopores in solid-state membranes can be made with user-defined dimensions, but chemical modifications require substantial effort.[10] A challenge in the field is to gain control over both the geometrical and chemical specifications of nanopores. We hypothesized that using DNA-based nanoplates as covers for solid-state nanopores could provide a route for meeting this challenge.

Our setup (Figure 1 a) consists of two electrolyte reservoirs separated by a silicon-supported free-standing insulating silicon nitride (SiN) membrane of thickness $L = 50$ nm. The membrane contains a single conical nanopore of diameter $D = 18$–25 nm (Figure 1 b), which is fabricated by electron beam lithography and reactive ion etching.[11] When a voltage is applied through the two electrodes, an ionic current flows through the nanopore and is recorded with a current amplifier. The dimensions and shape of the nanopore dominate the resistance of the setup. The *cis* side of the nanopore is covered with a rectangular nanoplate of width a, length b, and thickness l. The plate includes a central aperture of width x and length y (Figure 1 a). The nanoplates are produced by molecular self-assembly with scaffolded DNA origami (see the Supporting Information, note S1) and consist of a double layer of 46 tightly interlinked double-helical DNA domains in a honeycomb-type packing lattice. We made nanoplate versions (Supporting Information, Figures S1–S5) with a width and length of 50 nm, and a thickness of 6 nm. Correct formation of the nanoplates was confirmed using negative-stain transmission electron microscopy (Figure 1 b; see also the Supporting Information, notes S6–S9).

The nanoplates were electrically assembled onto the nanopores by injection into the *cis* electrolyte compartment. A sudden current drop and intensification in the current noise was typically observed within a few seconds (Figure 1 c) after the bias voltage was applied (Supporting Information, notes S2 and S3). The current blockades lasted for hours, unless reverse voltages were applied or the membrane was intensely rinsed. In both cases, the initial conductance level of the nanopore was restored. In experiments using nanopores with diameters exceeding the dimensions of the nanoplates, we observed transient blockades (Supporting Information, note S4), indicating that in those cases the nanoplates slipped through the larger nanopores. In experiments with membranes containing arrays of nanopores, we observed staircase-like decreases in conductivity (Supporting Information, Figure S12), indicating the progressive capture of nanoplates by individual nanopores in the array.

We find that, for nanoplates with apertures the conductance of nanoplate-on-nanopore hybrids decreases with decreasing aperture size (Figure 1 d). This finding can be explained by a model in which the nanoplates cover the nanopore in a flat orientation. Orthogonal or random orientations should yield relative conductances that do not depend on the size of the apertures. The nanopore conductance drops by approximately 17 % when using nanoplates lacking a central aperture. The DNA nanoplates are expected to be permeable to ions, owing to a mesh of vertical and horizontal channels. The vertical channels are formed by cavities between neighboring double-helical DNA domains between crosslinks along the helical axis,[4,5,12] while the horizontal channels are intrinsic to the honeycomb-type architecture of the DNA nanoplate. The corrugated lower surface of a nanoplate may provide additional channels for ion flow when it covers a nanopore.

The equivalent circuit model depicted in Figure 1 e,f accounts for the conductances of the bare nanopore (G_{pore}), the nanoplate (G_{plate}), and the central aperture ($G_{aperture}$). $G_{aperture}$ can be estimated for a given aperture size by a geometrical conductance model (Supporting Information, note S5). The value of G_{plate} can therefore be computed from the measured hybrid conductance. We evaluated G_{plate} versus G_{pore} for nanopores with diameters in the range of $D = 18$–25 nm and found that the conductance G_{plate} of the nanoplates increases linearly with the conductance G_{pore} of the nanopore

[*] R. Wei,[+] U. Rant
Walter Schottky Institute, Technische Universität München
Am Coulombwall 4, 85748 Garching near Munich (Germany)
E-mail: rant@tum.de
T. G. Martin,[+] H. Dietz
Center for Integrated Protein Science München & Institute for Advanced Study, Physics Department, Technische Universität München
Am Coulombwall 4a, 85748 Garching near Munich (Germany)
E-mail: dietz@tum.de
[+] These authors contributed equally to this work.

[**] This work was supported by the German Excellence Initiative through grants from the Nano Initiative Munich and from the Center for Integrated Protein Science Munich, by the Collaborative Research Center SFB 863 of the German Research Society (DFG), the TUM Institute for Advanced Study, and a European Research Council Starting Grant to HD. R.W. was supported by the TUM Graduate School's Faculty Graduate Center of Physics. Discussions with Friedrich Simmel, Michael Mayer, Daniel Branton, and George Church are gratefully acknowledged.

Supporting information for this article is available on the WWW under http://dx.doi.org/10.1002/anie.201200688.

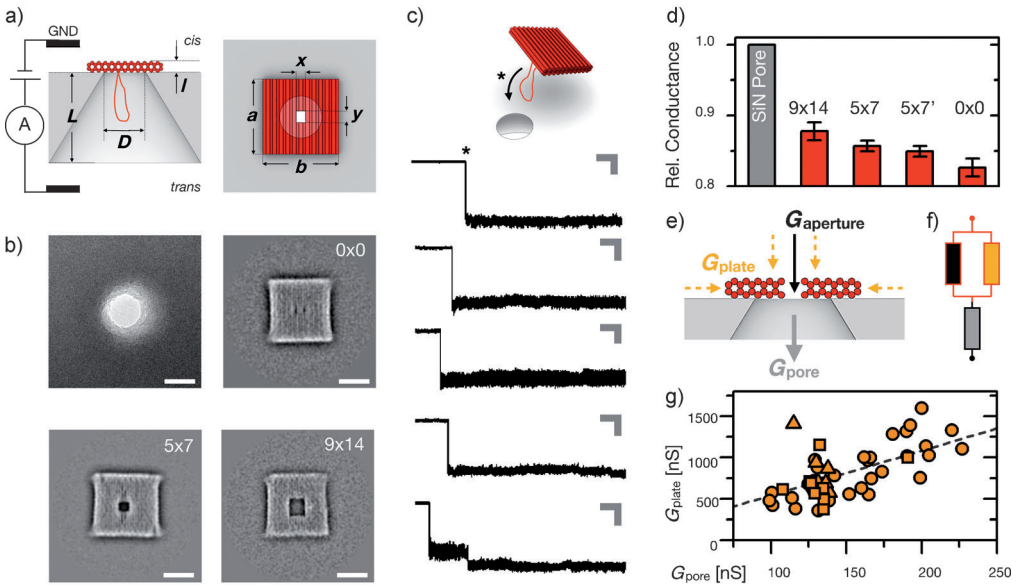

Figure 1. DNA nanoplates on SiN nanopores. a) Schematic of the experimental setup. The free-standing SiN membrane is shown in grey, the DNA nanoplate is shown in red. Inspired by previous work,[10d] we included a ca. 1300 base long single-stranded or double-stranded DNA loop that protrudes near the central aperture (see Figures S1-S5 for design details) to facilitate insertion into the nanopore. b) Top left: Transmission electron micrograph (TEM) of a bare nanopore. Top right and bottom row: average of aligned negative-stain TEM micrographs of nanoplates with varying aperture sizes (inset numbers indicate aperture width × length in nm) imaged separately on thin carbon support layers (Figures S6–S9). Scale bars: 20 nm. c) Nanoplates were injected at dilute effective concentrations of ca. 30 pmol L^{-1} with bias voltages of up to +200 mV applied to the *trans* electrode and captured electrically on nanopores. Horizontal scale bars: 2 s; Vertical scale bars: 10 nS. Asterisk marks nanoplate capture event. d) Relative conductance of nanplate-on-nanopore hybrids compared to conductance of bare nanopore before nanoplate insertion. Inset numbers indicate width × length in nm of a central aperture in the nanoplates; 5 × 7′ indicates a nanoplate version with one single-stranded DNA heptanucleotide overhang in the aperture (Figure S2). e, f) Schematic current paths and equivalent circuit model for the conductance of the nanoplate-on-nanopore hybrid. g) Nanoplate conductance G_{plate} correlates linearly with the conductance of the underlying nanopore G_{pore} (note S5); □ no aperture, ○ 5 nm × 7 nm aperture, and △ 9 nm × 14 nm aperture.

(Figure 1 g). Therefore, the area of the nanopore controls the area of the nanoplate that is exposed to ion flow. This finding agrees well with a geometric model (Supporting Information, note S5) that further supports the notion that the nanoplates cover the nanopore in the desired orientation. Neglecting potential ion fluxes that bypass the nanoplates, we estimate the transversal specific conductivity ($\sigma_{plate\perp}$) of the nanoplates to be $(7.8 \pm 0.4)\ S\,m^{-1}$ in an aqueous solution of KCl (1 M) and $MgCl_2$ (10 mM).

DNA nanoplates with custom apertures can serve as size-selective molecular gates for nanopores. To demonstrate this option, we added streptavidin (52 kDa, hydrodynamic diameter ca. 6 nm)[13] to the *cis* compartment of the nanopore setup along with nanoplates containing a central aperture of width 9 nm and length 14 nm. Before insertion of a nanoplate onto the nanopore, we observed sparse sub-millisecond current blockades caused by streptavidin molecules translocating through the bare nanopore (Figure 2 b). After nanoplate insertion, the current blockades caused by streptavidin translocation through the nanoplate-on-nanopore persisted (Figure 2 b, c; see also the Supporting Information, note S6). When we repeated these experiments with a significantly larger protein, immunoglobulin G (IgG, 150 kDa, effective hydrodynamic diameter ca. 14 nm), we found that with a nanoplate in place, IgG translocation was inhibited

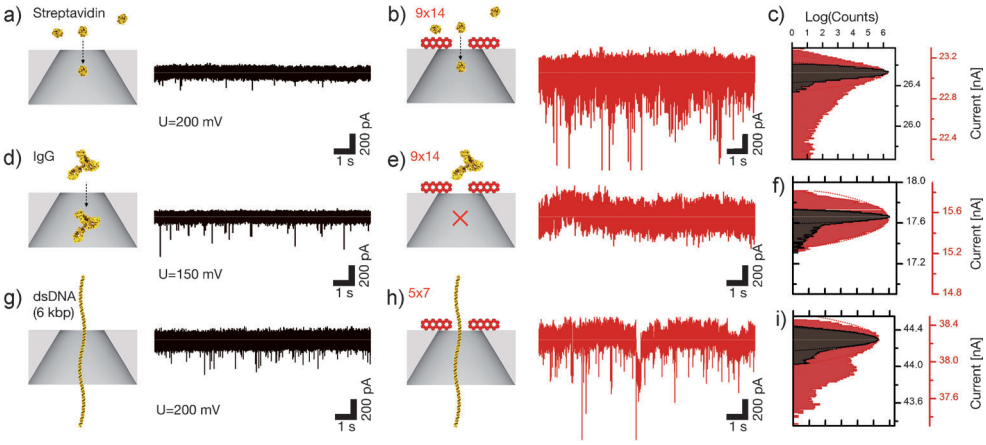

Figure 2. DNA nanoplates with custom apertures for size-selective macromolecular sensing with SiN nanopores. a) Current–time traces observed for streptavidin (*cis* concentration = 20 nM) translocation through bare nanopores, b) Current–time traces after insertion of a nanoplate with a central aperture of width 9 nm and length 14 nm (see Figure S5 for design details). c) Histogram of observed current levels. d–f) As in (a)–(c), but with Immunoglobulin G (IgG; *cis* concentration = 20 nM). g–i) As in (a)–(c), but with 6 kbp linear double-helical DNA molecules (*cis* concentration = 300 pM) and a nanoplate with aperture width 5 nm and length 7 nm (Figure S2, version 0).

(Figure 2d–f). The DNA nanoplates can also be applied for translocation experiments with double-stranded DNA molecules, as seen in experiments with linear DNA fragments 6000 base pairs long and nanoplates that include a central 5 nm × 7 nm aperture (Figure 2g–i; see also the Supporting Information, note S7). In experiments with a closed nanoplate, we did not detect DNA translocation (Supporting Information, note S8).

DNA nanoplates can also provide chemical selectivity for solid-state nanopores. To demonstrate this capability, we included chemical bait modifications within the nanoplate apertures to detect prey molecules that can selectively adhere to the bait (Figure 3a). The nanoplates thus become gatekeepers that can delay the passage of a target molecule through the aperture. In our experiments, we used single-stranded DNA motifs protruding from the double-helical DNA domains that form the boundary of the nanoplate aperture as bait (for design details, see Figures S2 and S3 in the Supporting Information). It is important to note that many different chemical bait moieties beyond single-stranded DNA can be conjugated in a site-directed fashion to a DNA nanoplate.

We performed translocation experiments using single-stranded DNA prey molecules with sequences $[T]_{24}CC[T]_{24}$ and $[T]_{23}CCGG[T]_{23}$ (Figures 3b–e) that can form at most two or four DNA base pairs, respectively, with a bait motif of sequence TTTCCGG located in the nanoplate aperture. Immediately after a nanoplate was assembled on the nanopore, we observed a continuous switching between two discrete current levels (Figure 3b,d). In the case of the $[T]_{24}CC[T]_{24}$ prey molecule, which can form at most two base pairs with the bait motif, we found that the current switching occurs much more quickly than in experiments with the $[T]_{23}CCGG[T]_{23}$ prey molecule, which can form four base pairs with the bait. We analyzed the distribution of the current blockade dwell times (Figures 3c,e) and found that the distributions can each be fit to a single exponential distribution. In the case of the $[T]_{24}CC[T]_{24}$ prey molecule, the average blockade dwell time was (41 ± 3) ms, while for $[T]_{23}CCGG[T]_{23}$ we found a value of (487 ± 28) ms. Differences in the binding energies, which in this case are controlled by the number of base pairs formed between prey and bait motifs, will be reflected in the bond lifetimes. We expected the characteristic dissociation time for the two prey motifs to differ by approximately a factor of $e^2 = 7.4$, which is close to what we observed. Therefore, the short bait motif in the nanoplate delays the translocation of single-stranded DNA molecules in a sequence-dependent fashion.

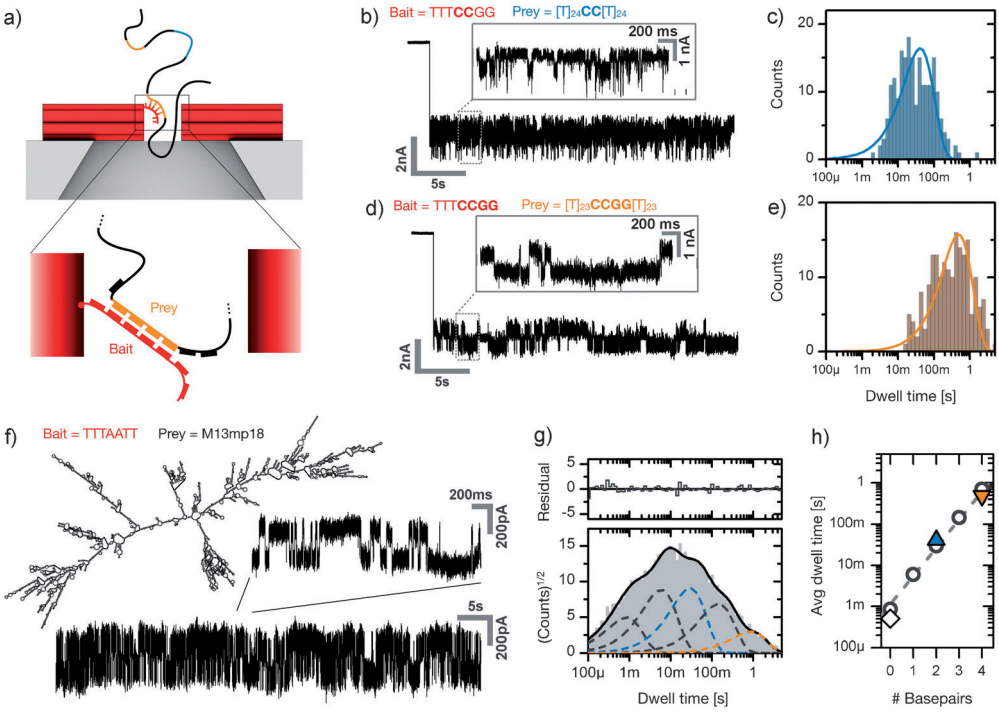

Figure 3. Sequence-specific prey DNA detection with functionalized DNA nanopores on SiN nanopores. a) Molecular bait is displayed in the nanoplate aperture (see Figures S2 and S3 for detailed implementation). b) Current–time trace observed in translocation experiments with an aperture-bound bait sequence TTTCCGG and a single-stranded prey molecule of sequence $[T]_{24}CC[T]_{24}$ (*cis* concentration = 300 pM). c) Bars: logarithmically binned histogram (N = 233) of current blockade dwell times. Solid line: single-exponential distribution (note S11). d, e) Results as in (b), (c), but obtained with prey sequence $[T]_{23}CCGG[T]_{23}$. Histogram includes N = 193 dwells. f) Current–time traces observed in translocation experiments with M13mp18 genomic DNA (*cis* concentration = 100 pM) and a nanoplate with bait motif TTTAATT (Figure S2, version 1). Inset shows a secondary structure map computed with Mfold.[14] g) Bars: histogram of logarithmically binned current blockade dwell times (N = 6100). Solid line: fit to a sum of five single exponentials (note S11). Dashed lines: individual single exponentials in the sum. h) ○ average dwell time τ_i from (g) sorted according to magnitude. ◇ average dwell time observed in translocation experiments with M13mp18 without bait motif (note S9, Figure S17). △, ▽ average dwell times τ found in (c; △) and (e; ▽).

Exposing nanoplates with bait motifs to more complex patterns of prey motifs yields current dwells that are distributed in a multi-exponential fashion with multiple characteristic time constants. To demonstrate this, we used the 7249 base long genome of the bacteriophage M13mp18, which can adopt complex secondary structures with many loop-terminated hairpins, as our prey molecule. One of many ground state structures with similar energies (as computed with Mfold)[14] to our experimental conditions is depicted in Figure 3f.

When the M13mp18 genome and nanoplates with a 5 nm × 7 nm central aperture lacking a bait motif were added to our nanopore setup, we observed transient current blockades with a short

characteristic time constant around 500 μs (Supporting Information, note S9). When a bait motif with sequence TTTAATT was included in the nanoplate aperture (Supporting Information, Figure S2), we observed current switching (Figure 3 f) between two defined levels. When this experiment was repeated with six bait motifs protruding into the nanoplate aperture, we observed multi-level current blockades (Supporting Information, Figure S3 and note S10). These observations suggest that the blockades are caused by excursions of segments of M13mp18 molecules, which may temporarily adhere to the bait motif, into the aperture. In the case of multiple bait motifs, several M13mp18 segments can dwell in the aperture simultaneously, thus explaining the multilevel blockades. In the absence of bait, the segments rapidly either retrocede or translocate.

We recorded several minute-long current–time traces and analyzed the statistical distribution of blockade dwells for the case of the M13mp18 genome as prey and a single bait with sequence TTTAATT in the nanoplate aperture. We found a dwell time distribution that is an additive superposition of five single exponential distributions (Figure 3 g; see also the Supporting Information, note S11). One of the five distributions has a time constant that matches the one found for the translocation of M13mp18 through a nanoplate lacking a bait sequence. Two of the five single exponential distributions have time constants that match those seen in Figure 3 c, e within a factor of two. Taken together, these findings suggest that the five characteristic dwell time constants reflect the dissociation of different types of duplexes formed between the bait and prey molecules (Figure 3 h). The time constants increase exponentially, suggesting that the duplexes formed differ by their length in base pairs. This theory is based on the assumption that duplex lifetimes grow exponentially with the number of base pairs formed.

In conclusion, we have presented DNA nanoplates that function with solid-state nanopores, which can be fabricated through standard electron beam lithography. The nanoplates are permeable to small ions, but the passage of macromolecules can be controlled by including custom apertures. The chemical addressability of the DNA nanoplates enables bait–prey single-molecule sensing experiments, as highlighted here by the sequence-specific detection of DNA snippets and genomic phage DNA. Applications in biomolecular interaction screens and for detecting DNA sequences by hybridization are readily conceivable. High-resolution sensing applications, such as electrical DNA sequencing will require reducing both the leakage current and current fluctuations.

Received: January 25, 2012
Published online: April 4, 2012

Keywords: DNA self-assembly · DNA structures · nanopores · nanotechnology · single-molecule studies

[1] N. C. Seeman, *Annu. Rev. Biochem.* **2010**, *79*, 65 – 87.
[2] a) E. Winfree, F. Liu, L. A. Wenzler, N. C. Seeman, *Nature* **1998**, *394*, 539 – 544; b) J. Zheng, J. J. Birktoft, Y. Chen, T. Wang, R. Sha, P. E. Constantinou, S. L. Ginell, C. Mao, N. C. Seeman, *Nature* **2009**, *461*, 74 – 77.
[3] P. W. K. Rothemund, *Nature* **2006**, *440*, 297 – 302.
[4] S. M. Douglas, H. Dietz, T. Liedl, B. Hogberg, F. Graf, W. M. Shih, *Nature* **2009**, *459*, 414 – 418.
[5] E. S. Andersen, M. Dong, M. M. Nielsen, K. Jahn, R. Subramani, W. Mamdouh, W. W. Golas, B. Sander, H. Stark, C. L. Oliveira, J. S. Pedersen, V. Birkedal, F. Besenbacher, K. V. Gothelf, J. Kjems, *Nature* **2009**, *459*, 73 – 76.
[6] a) H. Dietz, S. M. Douglas, W. M. Shih, *Science* **2009**, *325*, 725 – 730; b) D. Han, S. Pal, J. Nangreave, Z. Deng, Y. Liu, H. Yan, *Science* **2011**, *332*, 342 – 346.
[7] a) S. M. Douglas, J. J. Chou, W. M. Shih, *Proc. Natl. Acad. Sci. USA* **2007**, *104*, 6644 – 6648; b) M. J. Berardi, W. M. Shih, S. C. Harrison, J. J. Chou, *Nature* **2011**, *476*, 109 – 113; c) Y. Ke, S. Lindsay, Y. Chang, Y. Liu, H. Yan, *Science* **2008**, *319*, 180 – 183; d) R. J. Kershner, L. D. Bozano, C. M. Micheel, A. M. Hung, A. R. Fornof, J. N. Cha, C. T. Rettner, M. Bersani, J. Frommer, P. W. K. Rothemund, G. M. Wallraff, *Nat. Nanotechnol.* **2009**, *4*, 557 – 561; e) N. A. Bell, C. R. Engst, M. Ablay, G. Divitini, C. Ducati, T. Liedl, U. F. Keyser, *Nano Lett.* **20112**, *12*, 512 – 517.
[8] a) G. M. Church, D. W. Deamer, D. Branton, R. Baldarelli, J. Kasianowicz, US patent 5,795,782, **1995**; b) J. J. Kasianowicz, E. Brandin, D. Branton, D. W. Deamer, *Proc. Natl. Acad. Sci. USA* **1996**, *93*, 13770 – 13773; c) S. Howorka, Z. Siwy, *Chem. Soc. Rev.* **2009**, *38*, 2360 – 2384; d) B. M. Venkatesan, R. Bashir, *Nat. Nanotechnol.* **2011**, *6*, 615 – 624.
[9] a) L. Q. Gu, O. Braha, S. Conlan, S. Cheley, H. Bayley, *Nature* **1999**, *398*, 686 – 690; b) L. Movileanu, S. Howorka, O. Braha, H. Bayley, *Nat. Biotechnol.* **2000**, *18*, 1091 – 1095; c) S. Howorka, S. Cheley, H. Bayley, *Nat. Biotechnol.* **2001**, *19*, 636 – 639; d) J. Clarke, H. C. Wu, L. Jayasinge, A. Patel, S. Reid, H. Bayley, *Nat. Nanotechnol.* **2009**, *4*, 265 – 270; e) F. Olasagasti, K. R. Lieberman, S. Benner, G. M. Cherf, J. M. Dahl, D. W. Deamer, M. Akeson, *Nat. Nanotechnol.* **2010**, *5*, 798 – 806.
[10] a) Z. Siwy, L. Trofin, P. Kohli, L. A. Baker, C. Trautmann, C. R. Martin, *J. Am. Chem. Soc.* **2005**, *127*, 5000 – 5001; b) S. M. Iqbal, D. Akin, R. Bashir, *Nat. Nanotechnol.* **2007**, *2*, 243 – 248; c) S. Ding, C. Gao, L. Q. Gu, *Anal. Chem.* **2009**, *81*, 6649 – 6655; d) A. R. Hall, A. Scott, D. Rotem, K. K. Mehta, H. Bayley, C. Dekker, *Nat. Nanotechnol.* **2010**, *5*, 874 – 877; e) E. C. Yusko, J. M. Johnson, S. Majd, P. Prangkio, R. C. Rollings, J. Li, J. Yang, M. Mayer, *Nat. Nanotechnol.* **2011**, *6*, 253 – 260; f) S. W. Kowalczyk, L. Kapinos, T. R. Blosser, T. Magalhaes, P. van Nies, R. Y. Lim, C. Dekker, *Nat. Nanotechnol.* **2011**, *6*, 433 – 438; g) R. Wei, V. Gatterdam, R. Wieneke, R. Tampé, U. Rant, *Nat. Nanotechnol.* **2012**, DOI: 10.1038/NNANO.2012.24.
[11] R. Wei, D. Pedone, A. Zürner, M. Döblinger, U. Rant, *Small* **2010**, *6*, 1406 – 1414.
[12] C. E. Castro, F. Kilchherr, D. N. Kim, E. L. Shiao, T. Wauer, P. Wortmann, M. Bathe, H. Dietz, *Nat. Methods* **2011**, *8*, 221 – 229.
[13] M. Firnkes, D. Pedone, J. Knezevic, M. Döblinger, U. Rant, *Nano Lett.* **2010**, *10*, 2162 – 2167.
[14] M. Zuker, *Nucleic Acids Res.* **2003**, *31*, 3406 – 3415.

